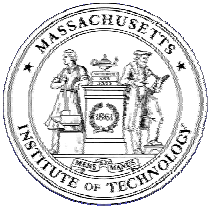


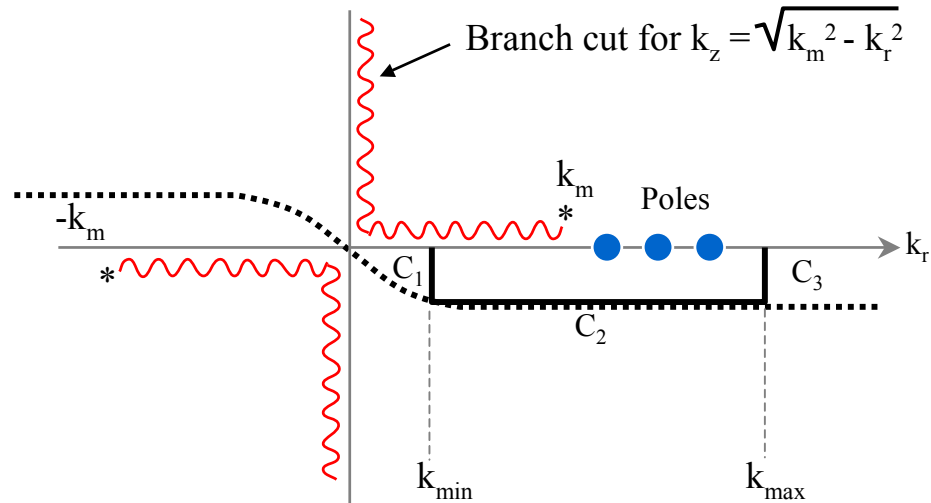
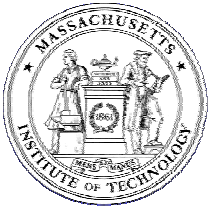
Computational Ocean Acoustics

- Ray Tracing
- Wavenumber Integration
- Normal Modes
- Parabolic Equation



Wavenumber Integration

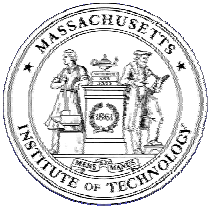
- Range-independent – Integral Transform solution
- Exact depth-dependent solution
 - Global Matrix Approach
 - Propagator Matrix Approach
 - Invariant Embedding
- Numerical Integration
 - Fast-Field Program (FFP)
 - Fast Hankel Transform
- Numerical issues:
 - Numerical stability of depth solution
 - Aliasing and wrap-around
- Numerical Examples



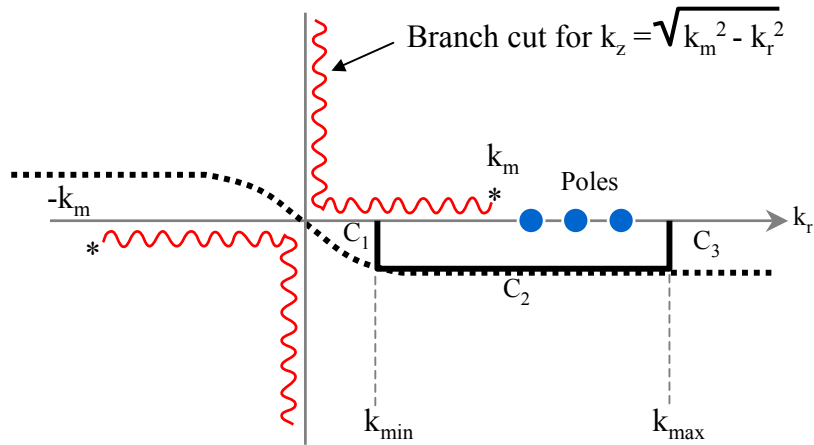
Complex integration contours for evaluation of wavenumber integral. The contour C2 is used for FFP integration, while the 'exact' hyperbolic tangent contour indicated by the dashed line is used for trapezoidal rule integration

Complex Contour Integration

$$\begin{aligned}
 g(r, z) &\simeq h(r) \int_C g(k_r, z) \sqrt{k_r} e^{ik_r r} dk_r, \\
 &\simeq h(r) \int_{k_{\min}}^{k_{\max}} g(k_r - i\epsilon, z) \sqrt{k_r - i\epsilon} e^{i(k_r - i\epsilon)r} dk_r.
 \end{aligned}$$



Complex Contour Integration



$$g(r, z) \simeq h(r) \int_C g(k_r, z) \sqrt{k_r} e^{ik_r r} dk_r,$$

$$\simeq h(r) \int_{k_{\min}}^{k_{\max}} g(k_r - i\epsilon, z) \sqrt{k_r - i\epsilon} e^{i(k_r - i\epsilon)r} dk_r.$$

$$g(r, z) e^{-\epsilon r} \simeq h(r) f(r, z) e^{-\epsilon r}$$

$$= h(r) \int_{k_{\min}}^{k_{\max}} g(k_r - i\epsilon, z) \sqrt{k_r - i\epsilon} e^{ik_r r} dk_r.$$

$$g^*(r_j, z) e^{-\epsilon r} = h(r_j) e^{ik_{\min} r_j} f^*(r_j, z) e^{-\epsilon r}$$

$$= h(r_j) \sum_{n=-\infty}^{\infty} f(r_j + nR, z) e^{-\epsilon(r_j + nR)}$$

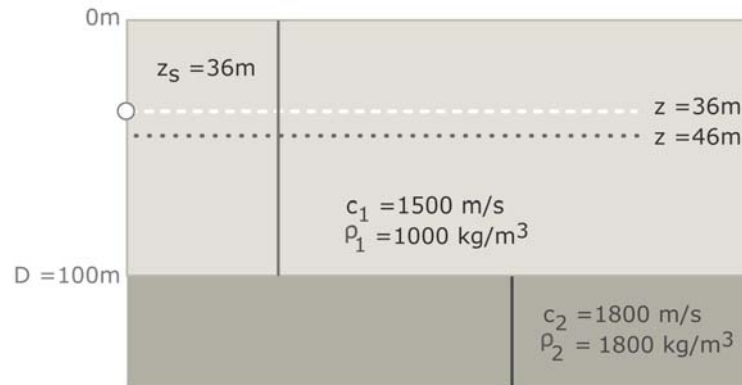
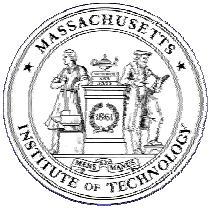
$$\simeq h(r_j) \Delta k_r e^{ik_{\min} r_j} \sum_{\ell=0}^{M-1} \left[g(k_{\ell} - i\epsilon, z) e^{ir_{\min} \ell \Delta k_r} \sqrt{k_{\ell} - i\epsilon} \right] e^{i \frac{2\pi \ell j}{M}},$$

$$g(r_j, z) \simeq h(r_j) f(r_j, z)$$

$$= e^{\epsilon r_j} h(r_j) \Delta k_r e^{ik_{\min} r_j} \sum_{\ell=0}^{M-1} \left[g(k_{\ell} - i\epsilon, z) e^{ir_{\min} \ell \Delta k_r} \sqrt{k_{\ell} - i\epsilon} \right] e^{i \frac{2\pi \ell j}{M}}$$

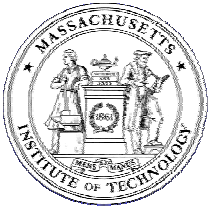
$$- h(r_j) \sum_{n \neq 0} f(r_j + nR, z) e^{-\epsilon n R}.$$

$$\epsilon = \frac{3}{R \log e} = \frac{3}{2\pi (M-1) \log e} (k_{\max} - k_{\min}),$$



Example: Pekeris waveguide with pressure-release surface and penetrable fluid bottom

See Fig 4.7 in Jensen, Kuperman, Porter and Schmidt.
Computational Ocean Acoustics. New York: Springer-Verlag, 2000.



Fast Hankel Transforms

$$\begin{aligned}g(r) &= \int_0^\infty g(k_r) k_r J_0(k_r r) dk_r \\ &= \frac{1}{2} \int_0^\infty g(k_r) k_r \left[H_0^{(1)}(k_r r) + H_0^{(2)}(k_r r) \right] dk_r\end{aligned}$$

FFP Asymptotics

$$\lim_{kr \rightarrow \infty} H_0^{(1,2)}(k_r r) = \sqrt{\frac{2}{\pi k_r r}} e^{\pm i[k_r r - \frac{\pi}{4}]},$$

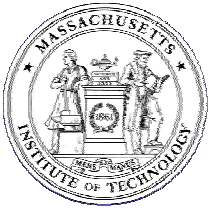
$$g(r) \simeq g^*(r) = \sqrt{\frac{1}{2\pi r}} \int_0^\infty g(k_r) \sqrt{k_r} \left[e^{i[k_r r - \frac{\pi}{4}]} + e^{-i[k_r r - \frac{\pi}{4}]} \right] dk_r$$

Fourier Transform Representation

$$g^*(r) = \int_{-\infty}^\infty f(k_r) e^{ik_r r} dk_r,$$

Integration kernel

$$f(k_r) = \begin{cases} g(-k_r) \sqrt{\frac{-k_r}{2\pi r}} e^{i\frac{\pi}{4}} & k_r < 0 \\ g(k_r) \sqrt{\frac{k_r}{2\pi r}} e^{-i\frac{\pi}{4}} & k_r \geq 0 \end{cases}$$



Fast Hankel Transform

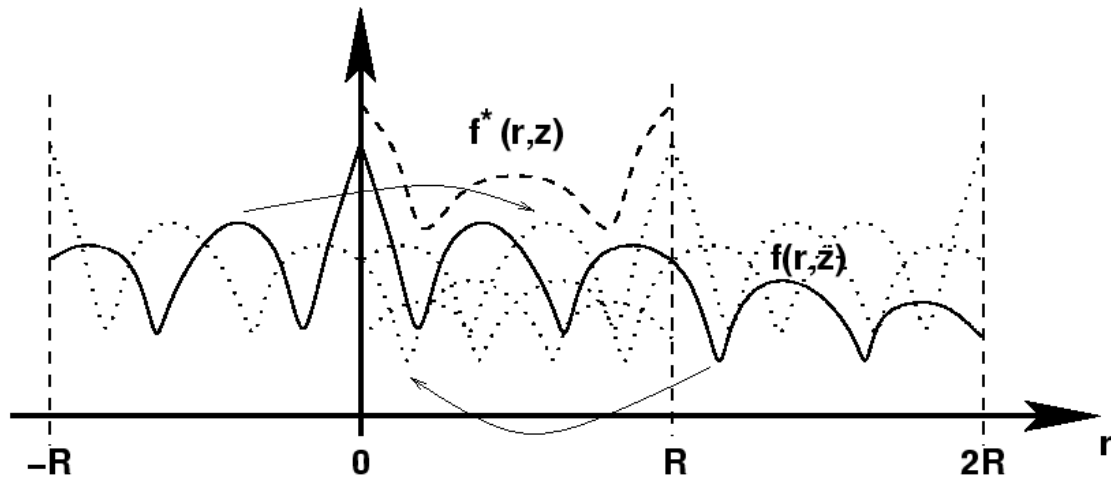
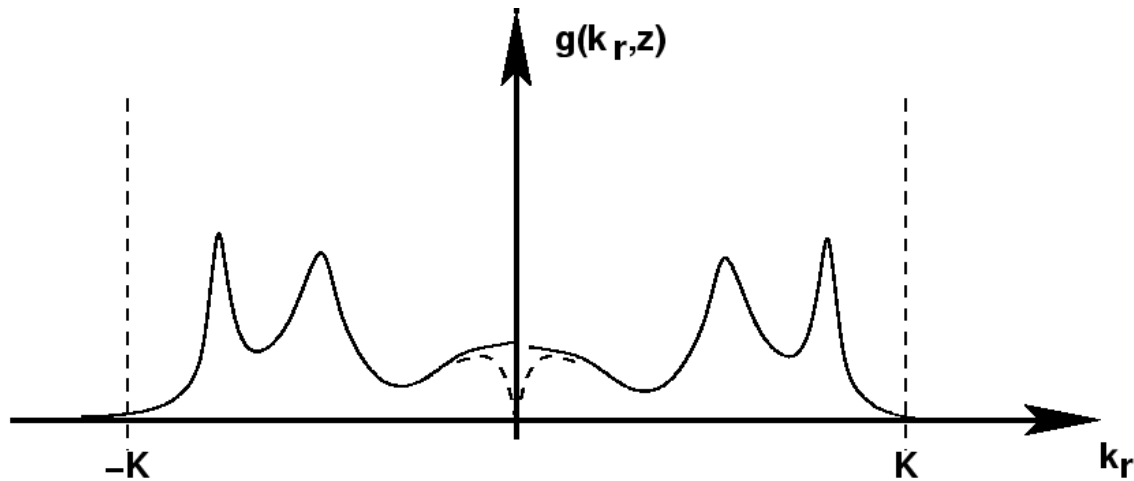
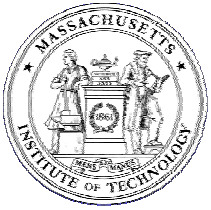
$$g(r) = g^*(r) + \int_0^{20\pi/r} g(k_r) w(k_r r) [k_r J_0(k_r r) - \sqrt{\frac{k_r}{2\pi r}} (e^{i(k_r r - \frac{\pi}{4})} + e^{-i(k_r r - \frac{\pi}{4})})] dk_r$$

Weight function

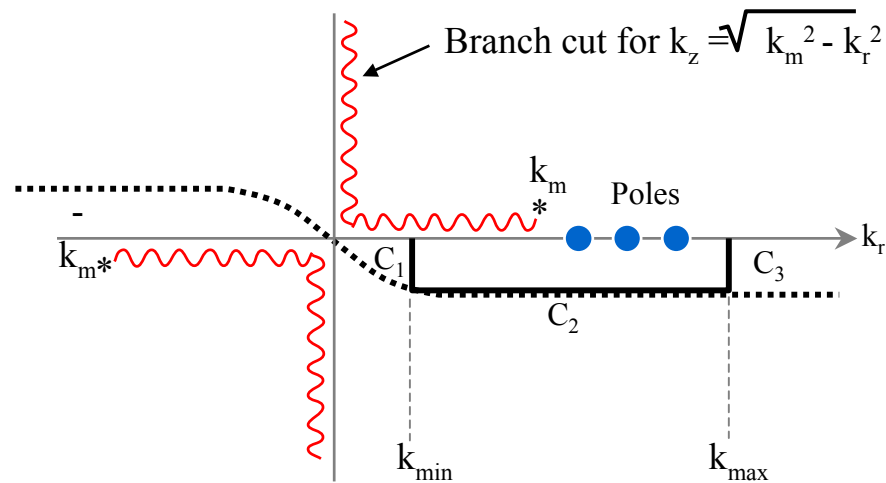
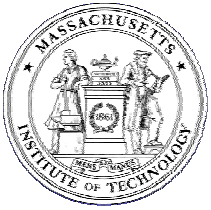
$$w(k_r r) = \begin{cases} 1 & k_r r \leq 10\pi \\ [1 + \cos(\pi(kr - 10\pi)/(10\pi))] / 2 & 10\pi < k_r r < 20\pi \end{cases}$$

Bessel Function Table

$$kr = n\Delta k_r \Delta r, \quad n = 0, \dots, 20\pi/(\Delta k_r \Delta r),$$



Aliasing associated with Fast Hankel Transform integration for typical Pekeris waveguide problem. The symmetric wavenumber kernel showing the presence of a two attenuated modes is sketched in the upper plot, with the $\sqrt{k_r}$ introduced by the FFP approximation indicated by the dashed curve near the origin. The discrete wavenumber integration yields the periodic result shown in the lower frame by a dashed curve, approximating the correct continuous result shown as a solid curve. The discrete result is a superposition of the 'true' field produced by the mirror sources in all the range windows.



Complex integration contours for evaluation of wavenumber integral. The contour C2 is used for FFP integration, while the 'exact' hyperbolic tangent contour indicated by the dashed line is used for trapezoidal rule integration

Trapezoidal Rule Integration

Wavenumber Discretization

$$\Delta k_r R < \frac{\pi}{4},$$

Exact Complex Contour

$$\bar{k}_r = \begin{cases} k_r(1 - i\epsilon \tanh k_r/6\Delta k_r), & k_r/6\Delta k_r \leq 20 \\ k_r(1 - i\epsilon), & k_r/6\Delta k_r > 20, \end{cases}$$



Hankel Transform Compensation

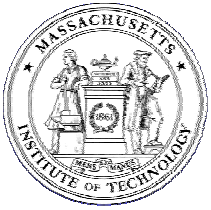
$$g(r) = \int_0^\infty g(k_r r) [w(k_r r) k_r J_0(k_r r) + (1 - w(k_r r)) \sqrt{\frac{k_r}{2\pi r}} (e^{i(k_r r - \frac{\pi}{4})} + e^{-i(k_r r - \frac{\pi}{4})})] dk_r ,$$

Weight function

$$w(k_r r) = \begin{cases} 1 & k_r r \leq 10\pi \\ [1 + \cos(\pi(k_r r - 10\pi)/(10\pi))] / 2 & 10\pi < k_r r < 20\pi \\ 0 & k_r r > 20\pi \end{cases}$$

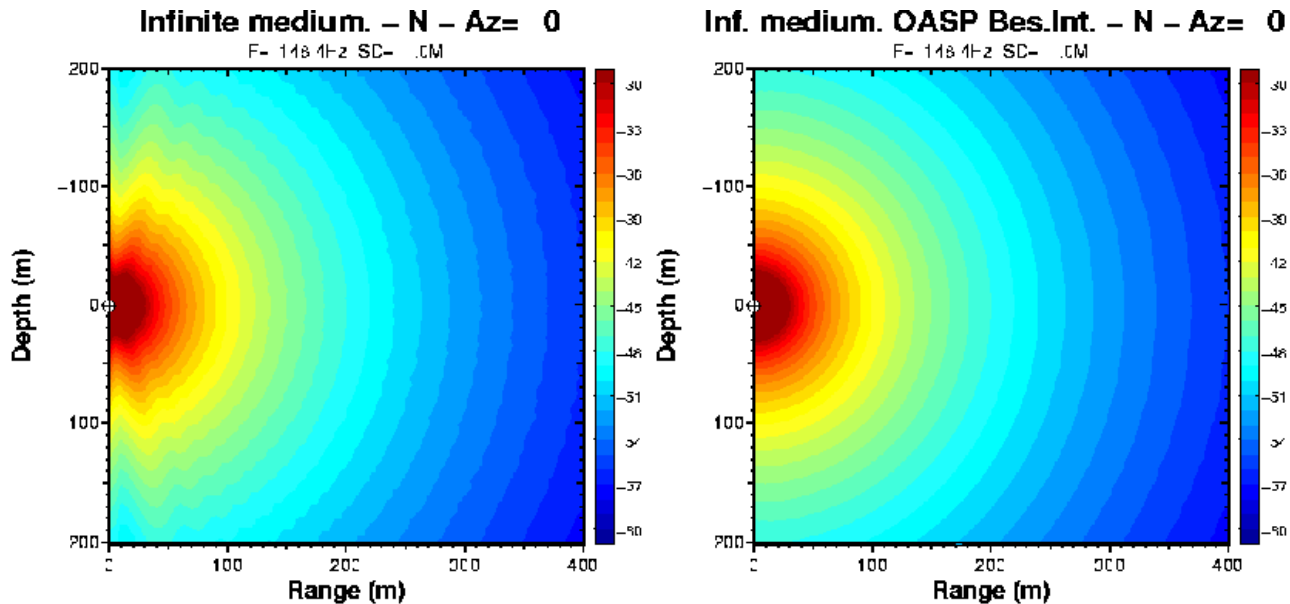
Numerical Implementation

- Use FFP approximation, evaluated either by direct numerical integration or FFT.
- Compute lookup table for $J_0(x)$, $x < 20\pi$ with $\simeq 40$ samples per period ($\simeq 400$) values.
- Modify $g(r, z)$ by a tapered difference between the Bessel function and of the asymptotic Hankel function for all values of $k_r r < 20\pi$.
- Computationally efficient by Lagrange interpolation in Bessel function lookup table.

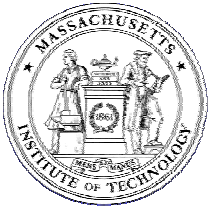


Example: Free space Green's function

p(r, z) = integral from 0 to infinity of (e^{ik_z|z|} / ik_z) * k_r * J_0(k_r r) dk_r



Acoustic point source field. (a) shows the FFP approximation which clearly breaks down at steep angles and short ranges, while (b) shows the correct spherical spreading behavior at all propagation angles, produced using Eq. (1)



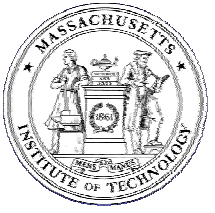
Filon Integration

$$\int_a^b f(k_r) e^{Sg(k_r)} dk_r = \begin{cases} \frac{\Delta k_r}{S \Delta g} \left[\Delta \{f e^{Sg}\} - \frac{\Delta f \Delta \{e^{Sg}\}}{S \Delta g} \right], & \Delta g \neq 0 \\ \frac{\Delta k_r}{2} \left[f(a) e^{Sg(a)} + f(b) e^{Sg(b)} \right], & \Delta g = 0, \end{cases}$$

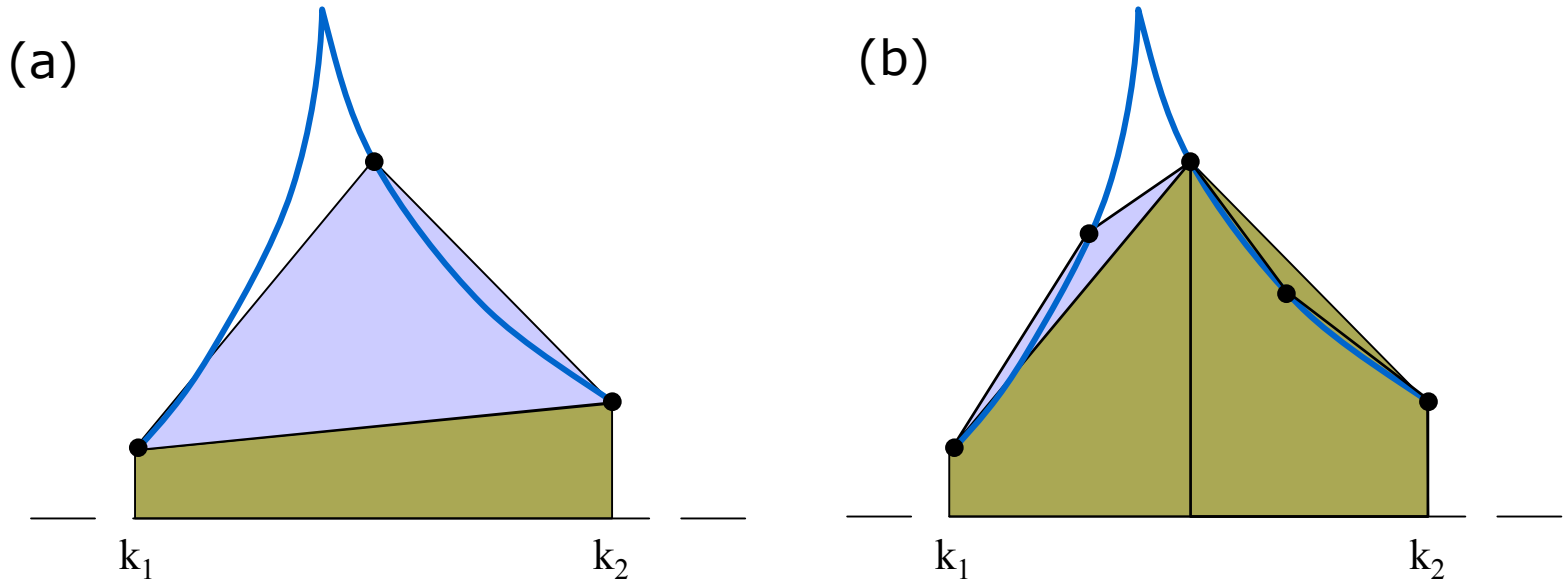
$$g(r_j, z) \simeq \frac{w_j}{\sqrt{2\pi r_j}} e^{i[k_{\min} r_j - \frac{\pi}{4}]} \sum_{\ell=0}^{M-1} \left[g(k_\ell, z) e^{i r_{\min} \ell \Delta k_r \sqrt{k_\ell}} \right] e^{i \frac{2\pi \ell j}{M}}.$$

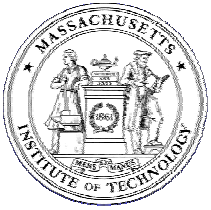
Range-dependent quadrature weights

$$w_j = \Delta k_r \left[\frac{\sin(\Delta k_r r_j / 2)}{\Delta k_r r_j / 2} \right]^2.$$



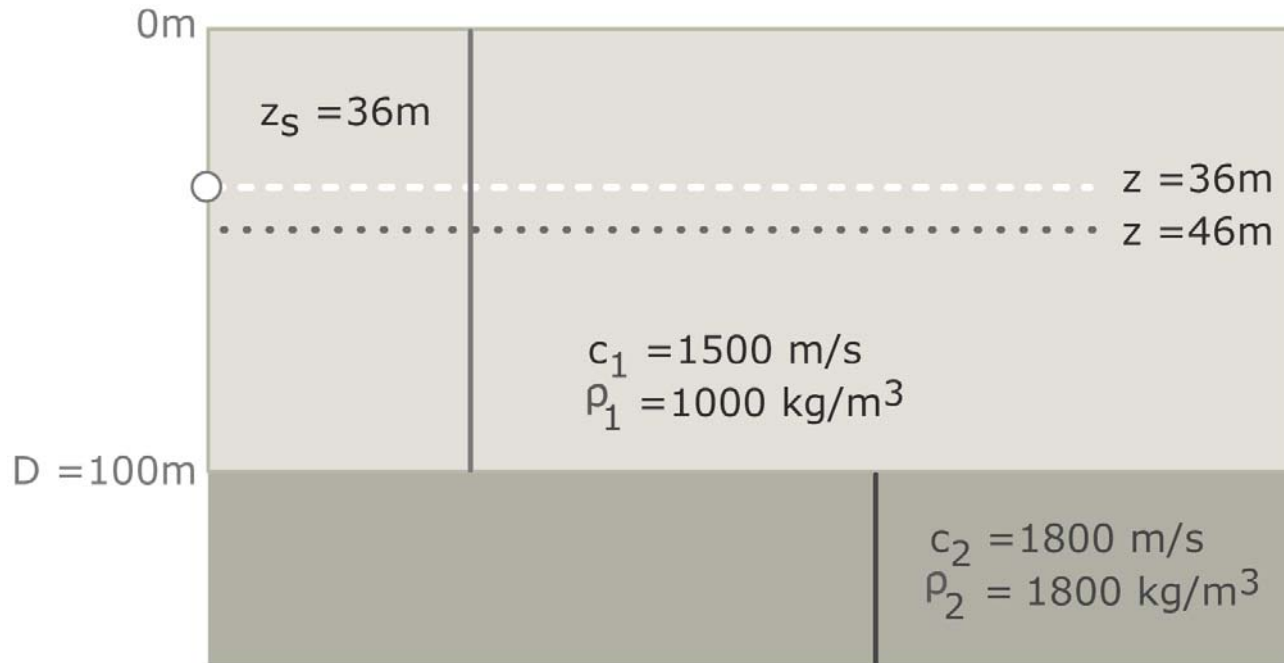
Adaptive Integration

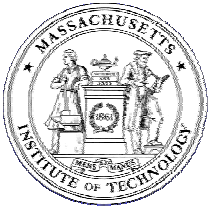




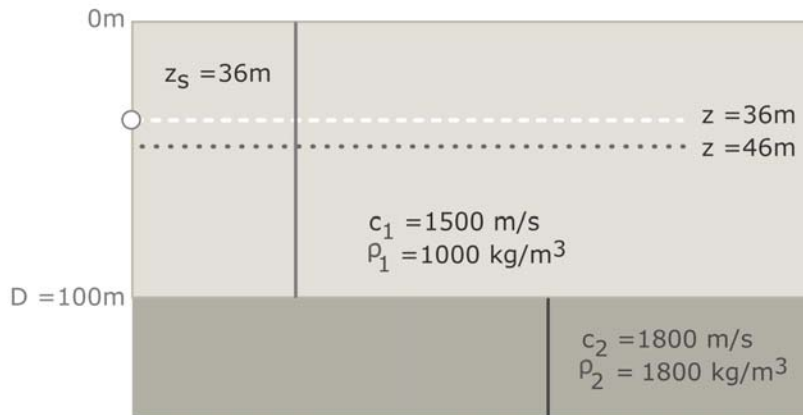
Numerical Examples

Pekeris Waveguide with Elastic Bottom



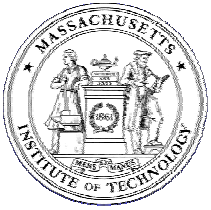


Shallow Water Waveguide with Fast Shear Bottom

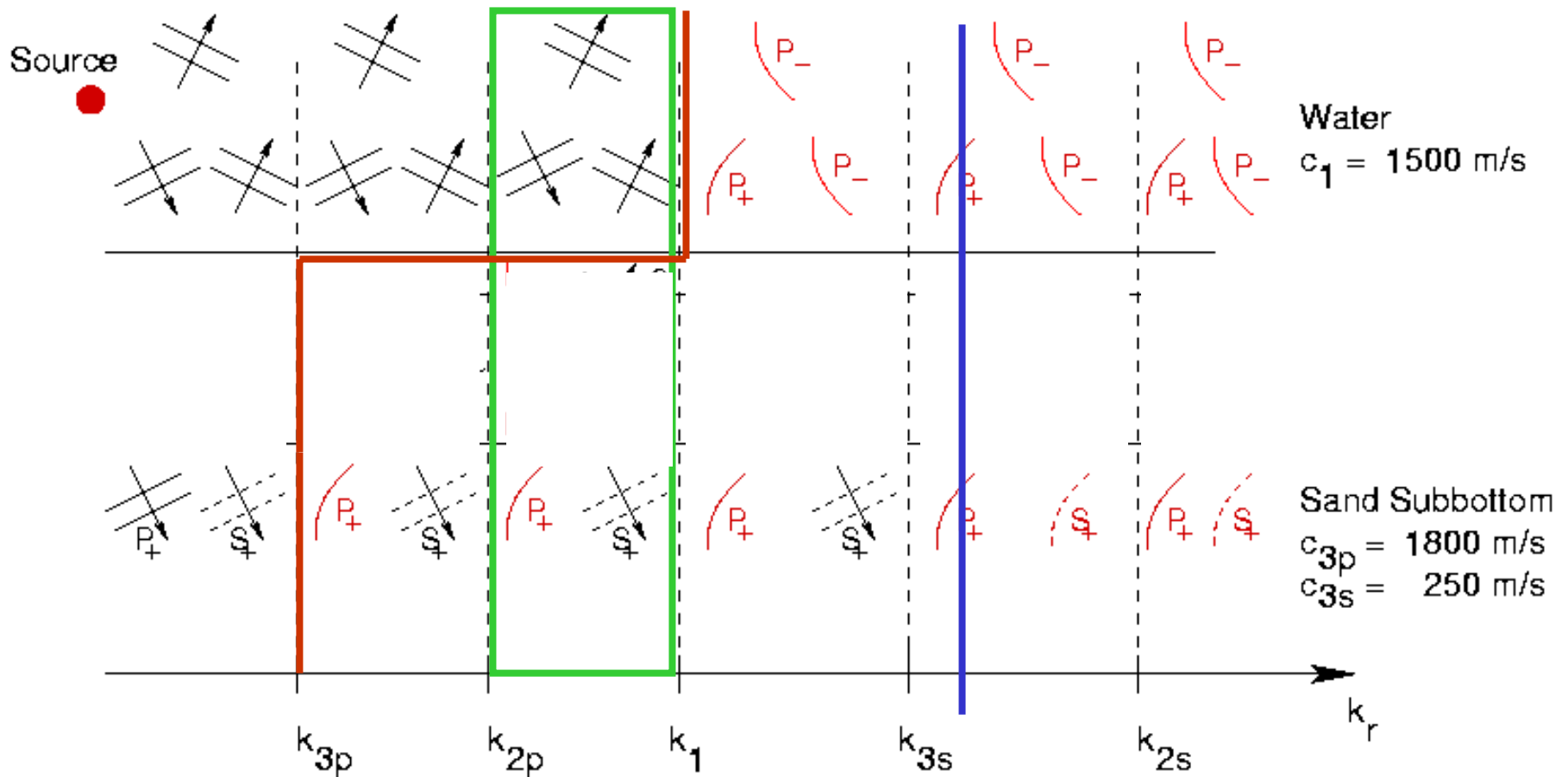


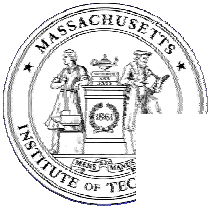
[See Jensen, Fig 4.9]

$$C_s = 600\text{ m/s}$$



Stratified Elastic Bottom Scholte wave – Fast Sand Seabed





Scholte Waves in Shallow Water

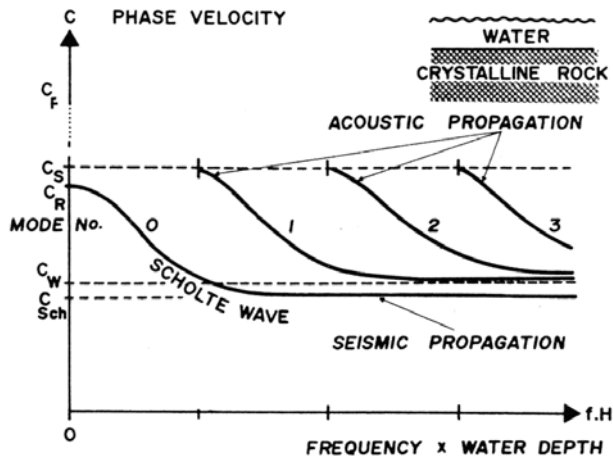


Fig. 1 Phase-velocities of the lowest modes in shallow water over an extremely "hard" rock-bottom

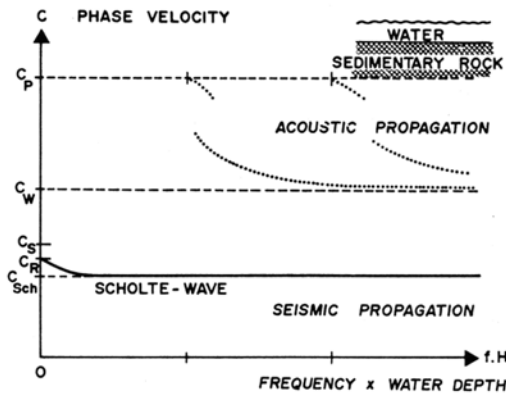


Fig. 2 Phase-velocities of the lowest modes in shallow water over a relative "soft" rock-bottom

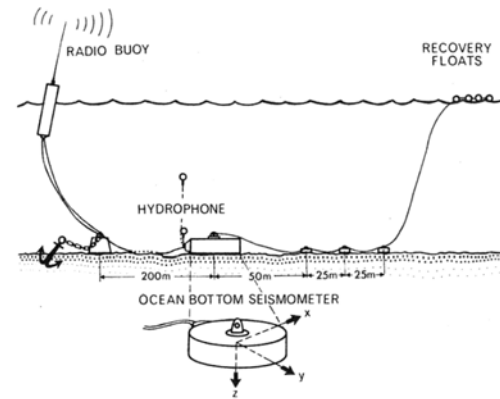


Fig. 8 Installation of the sensor package on the sea floor and mooring of its radio buoy in shallow water

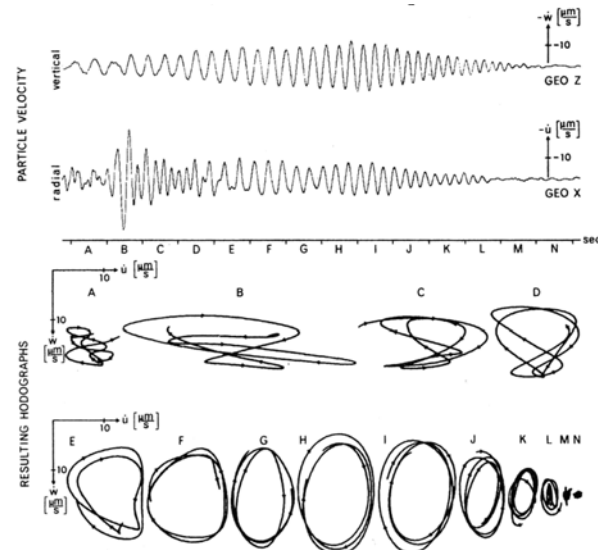
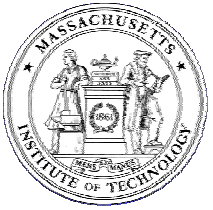


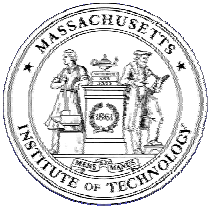
Fig. 12 Radial and vertical particle velocity of the interface wavelet in Fig. 11 with the resulting hodographs

Reproduced by permission from Rauch, Dieter, "Experimental and Theoretical Studies of Seismic Interface Waves in Coastal Waters." In *Bottom-Interacting Ocean Acoustics: NATO Conference Series, Marine Sciences*. Edited by William A. Kuperman & Finn B. Jensen. New York: Plenum Press, 1980.



Scholte Waves Inversion For Seabed Shear Properties

[See Jensen, Figs 8.9, 8.10, 8.11]

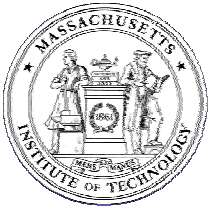


Seabed Shear Properties from Scholte Wave Inversions

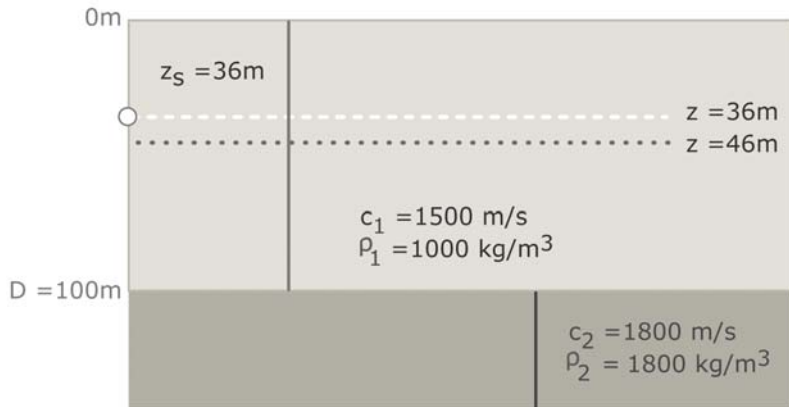
Table 1 Interface wave experiments

Investigators	Year	Water depth (m)	Bottom type	Centre freq. (Hz)	Measured att. (dB/km)	Inferred shear speed (m/s)	Inferred shear att. (dB/ λ_s)
Bucker, Whitney, Keir ⁶	1964	1 20	sand sand	20 25	300 200	100 195	1.4 1.4
Davies ⁷	1965	4410	-	6	-	50-190	-
Herron, Dorman, Drake ⁸	1968	5	silt	5	-	40-115	-
Hamilton et al. ⁹	1970	390 985	silt silt	- -	- -	100 90	- -
Schirmer ¹⁰	1980	130	sand	4.5	7	120	0.2
McDaniel, Beebe ¹¹	1980	32	sand	10	-	200	-
Essen et al. ¹²	1981	1	silt	4	-	75-250	-
Tuthill et al. ¹³	1981	7	mud	4.5	-	25-50	-
Whitmarsh, Lilwall ¹⁴	1982	5260	-	4.5	-	25-170	-
Holt, Hovem, Syrstad ¹⁵	1983	-	sand	35	600	135-195	2.3
Brocher et al. ¹⁶	1983	67	sand	5	0.43	260	0.02
Schmalfeldt, Rauch ¹⁷	1983	20 30	- -	3 3	10 2	100 150	0.3 0.1

Reproduced by permission from Jensen, Finn B. and Henrick Schmidt. "Shear Properties of Ocean Sediments Determined from Numerical Modelling of Scholte Wave Data." In Ocean Seismo-acoustics: Low Frequency Underwater Acoustics (NATO Conference Series, Marine Sciences). Edited by Tuncay Akal and Jonathan M. Berkson. New York: Plenum Press, 1986.

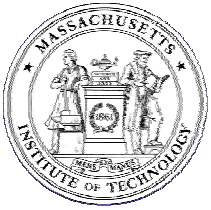


Shallow Water Waveguide with Slow Shear Bottom

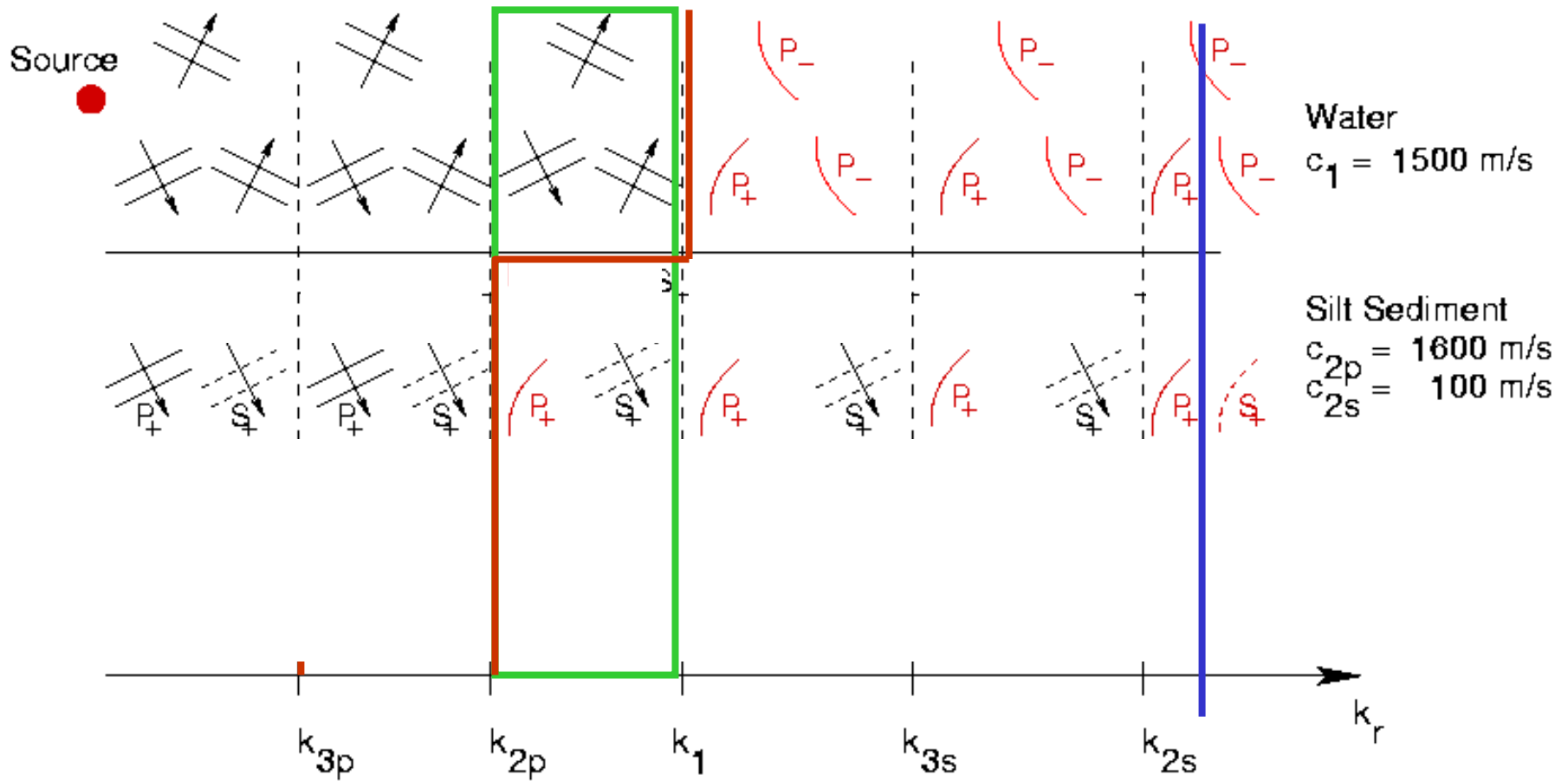


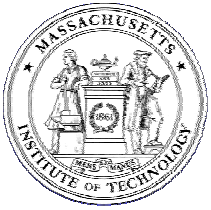
[See Jensen, Fig 4.10]

$$C_s = 300 \text{ m/s}$$

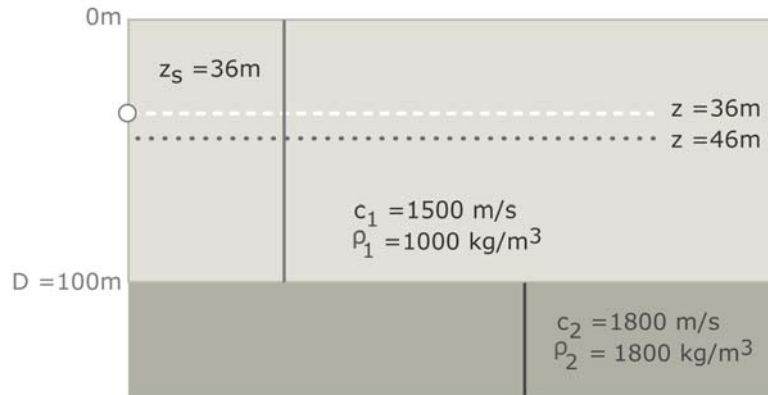


Stratified Elastic Bottom Scholte wave – Silt Seabed

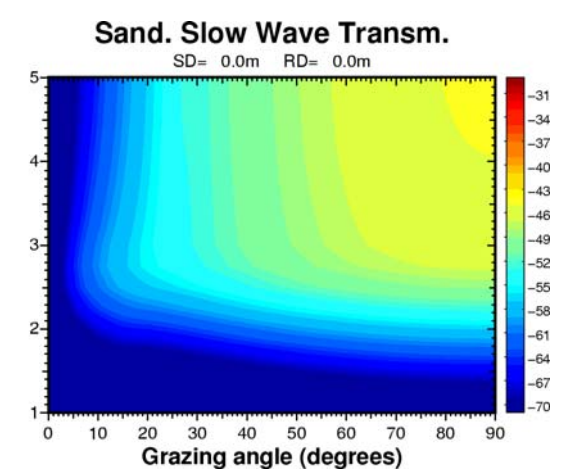
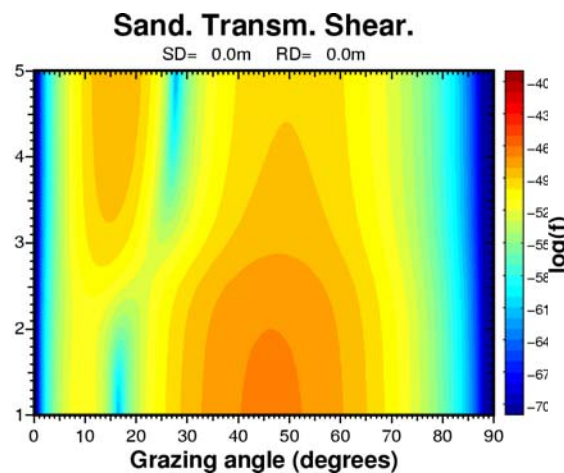
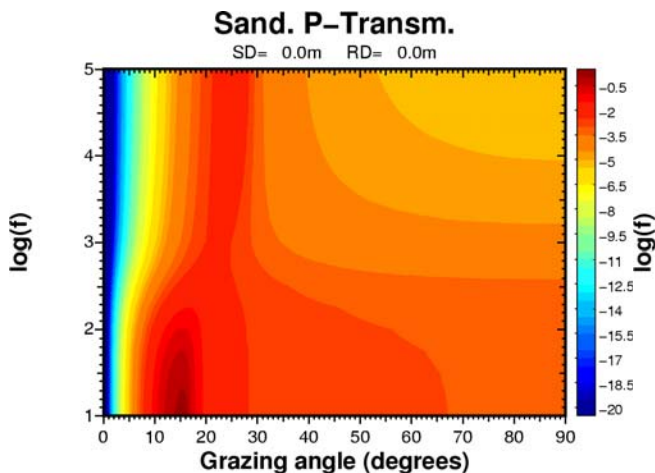
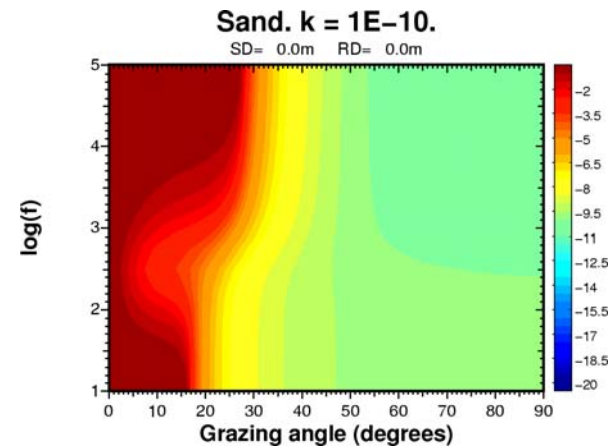


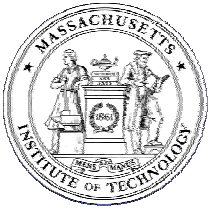


Shallow Water Waveguide with Porous, Unconsolidated Sand Bottom

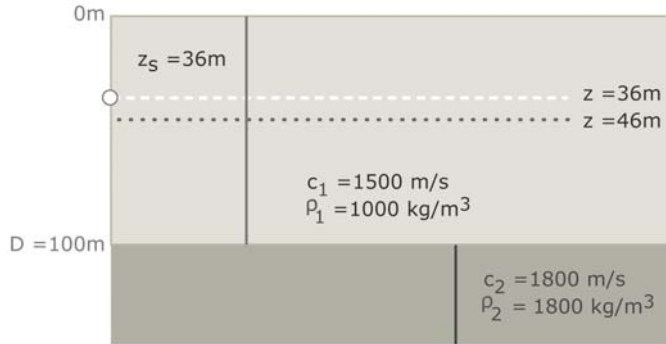


Porous Sand – Permeability $k = 10^{-10}$

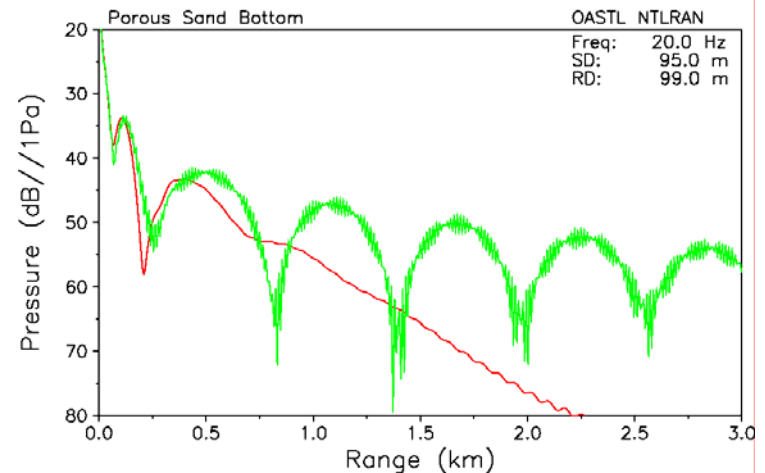
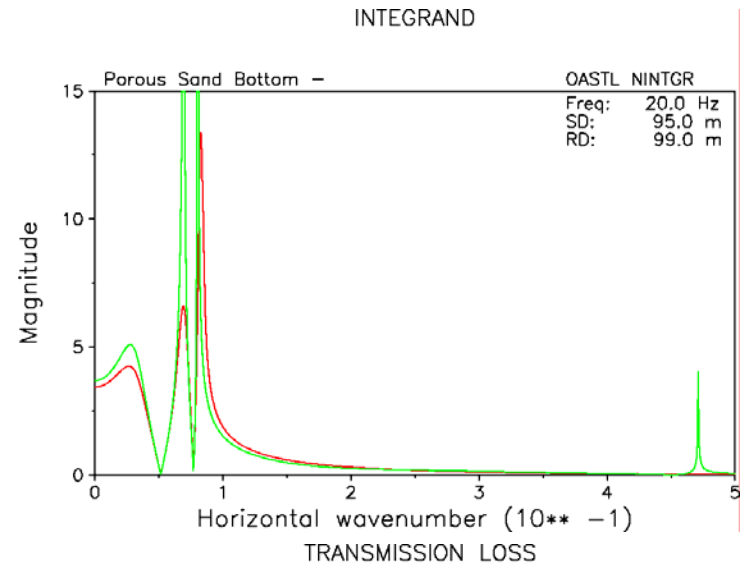


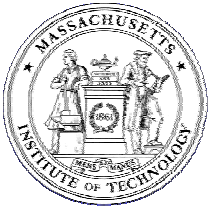


Shallow Water Waveguide with Porous, Unconsolidated Sand Bottom



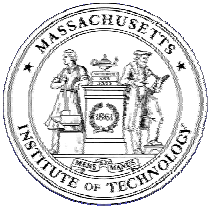
Porous Sand – Permeability $k = 10^{-10}$



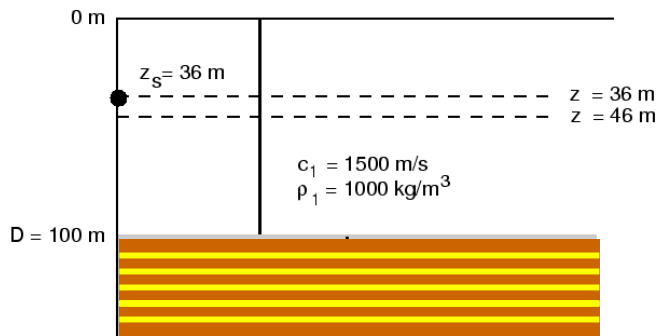


Seabed Dispersion Sand Seabed - Elba

See Maguer, Pouliquen, Bovio, Fox, and Schmidt.
"Comparison between subcritical penetration models and *in situ* data."
Journal of the Acoustical Society of America 103, no. 5 (May 1998): 2901.



Shallow Water Waveguide Transversely Isotropic Bottom

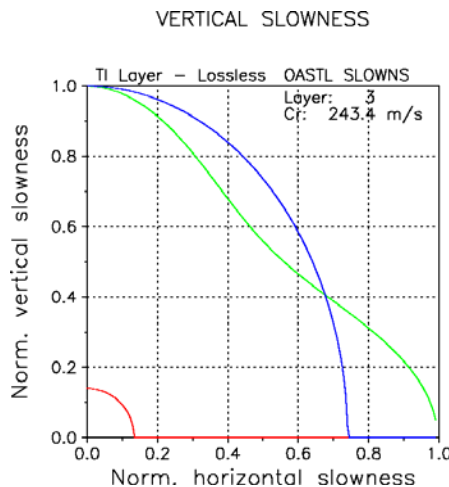


Silt 1600/200

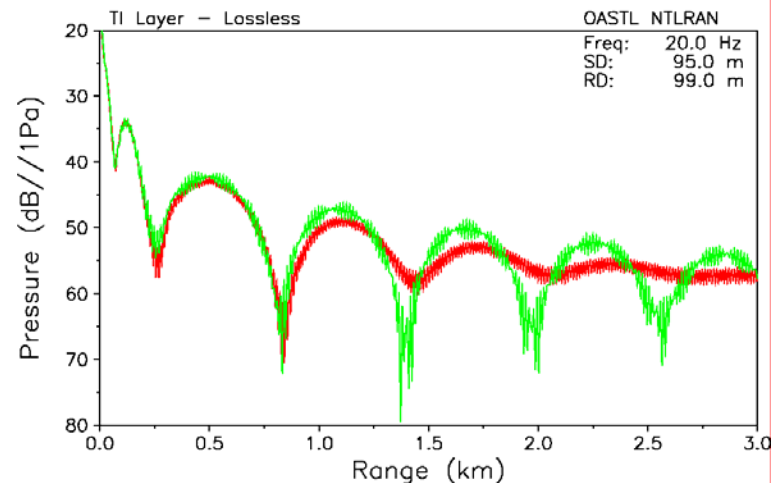
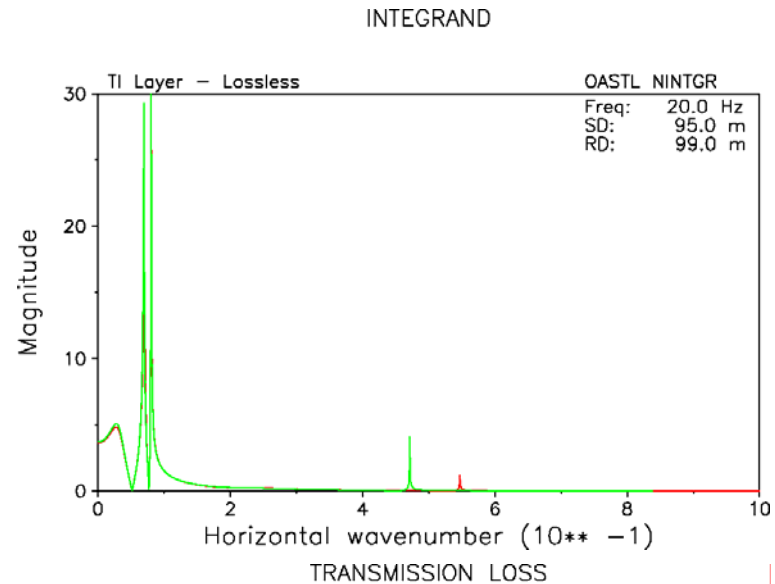
Sand 2000/400

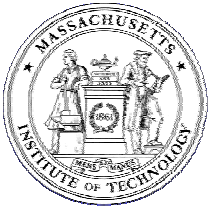
$$\langle C_p \rangle = 1800 \text{ m/s}$$

$$\langle C_s \rangle = 300 \text{ m/s}$$

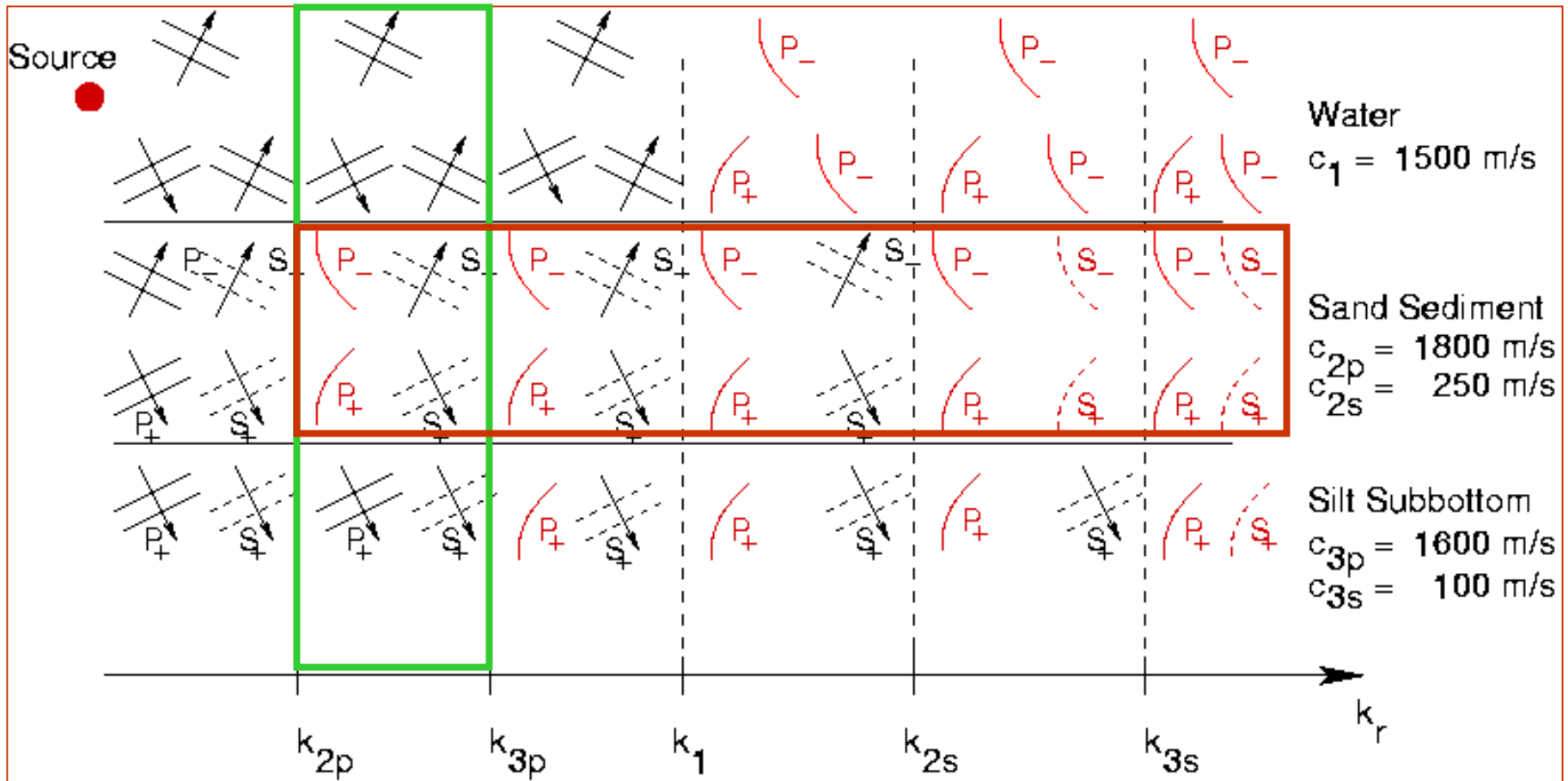


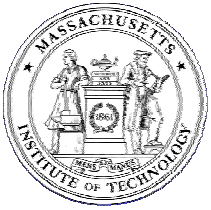
— P
— SV
— SH



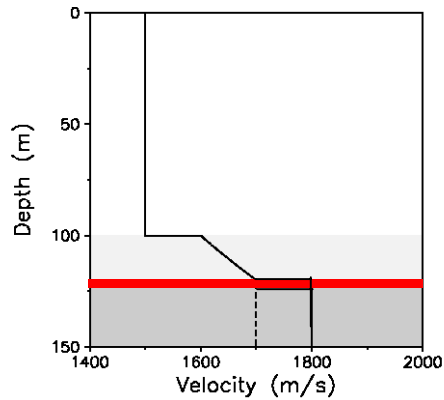


Stratified Elastic Bottom Evanescent Tunneling Regime



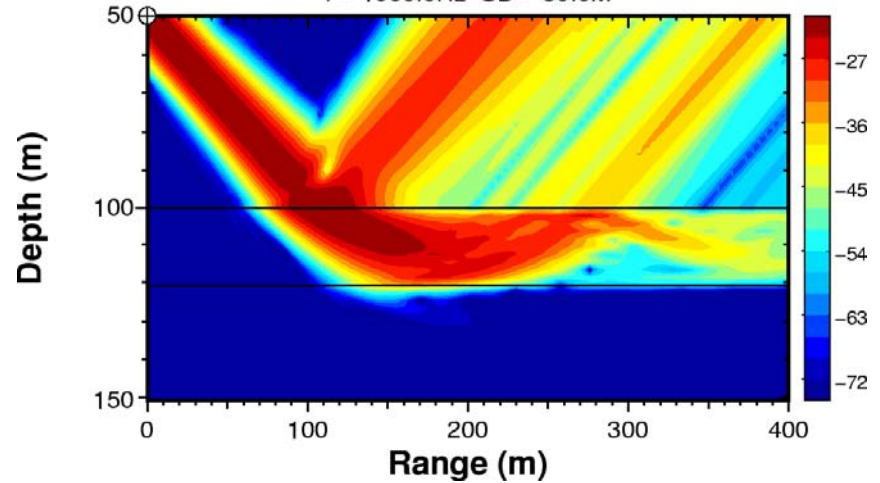


Evanesccent Wave Tunneling



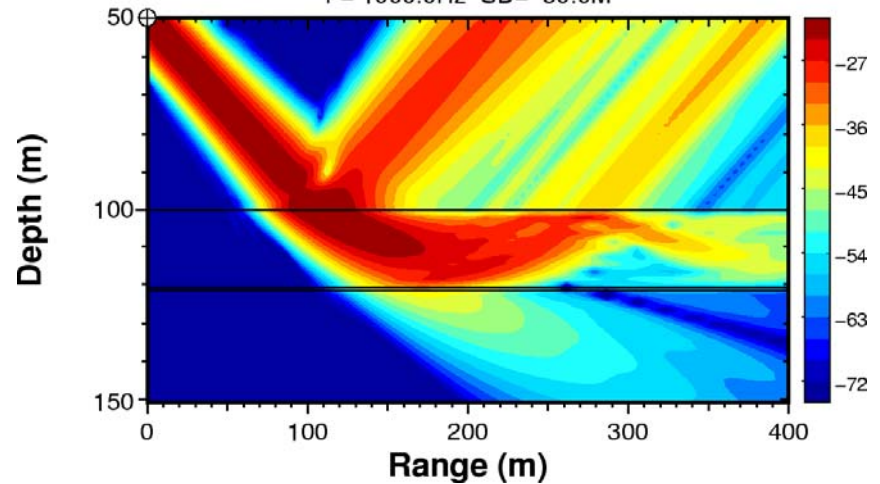
Beam

F= 1000.0Hz SD= 50.0M

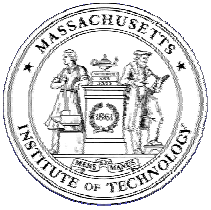


Beam tunnelling

F= 1000.0Hz SD= 50.0M



See Fig. 4.14 in Jensen, Kuperman, Porter and Schmidt. *Computational Ocean Acoustics*. New York: Springer-Verlag, 2000.



Shallow Water Seismo-Acoustics

- Bottom-limited Waveguide Propagation
 - Critical angles 15-25 degrees
 - Normal mode propagation characteristics for longer ranges
 - Branch line integral contribution significant for ranges $< 5-10 H$
 - Evanescent penetration and scattering dominant - tunneling
 - Wavenumber integration modeling 'exact' and decomposes into physically interpretable components
- Elasticity
 - Very low shear speeds $< 10-100$ m/s – makes shear a perturbative effect
 - Scholte waves dominating propagation mechanism below 10 Hz
- Porosity of sandy sediments
 - Strong dispersion in 1-10 kHz regime
- Transverse Isotropy
 - Seasonal sedimentation creates significant anisotropy (P: 10%, S: 30%)